Two-dimensional Bimetallic CoFe Selenite via Metal-ion Assisted Self-Assembly for Enhanced Oxygen Evolution Reaction

Ling-Li Zhou, Dong-Sheng Pan, Zheng-Han Guo and Jun-Ling Song*

International Joint Research Center for Photoresponsive Molecules and Materials, School of Chemical and Material Engineering, Jiangnan University, Lihu Street 1800, Wuxi 214122, China.

*Corresponding Author. E-mail: s070054@e.ntu.edu.sg

Physical Characterization

Single crystal X-ray diffraction was performed on a Bruker D8 VENTURE X-ray diffractometer. Powder X-ray diffraction (PXRD) patterns were collected recorded by Bruker D8 instrument with Cu-Kα radiation (λ = 1.5406 Å); the spectra were recorded in the 2θ range of 5° to 50°. The morphologies were characterized by a Hitachi S4800 microscope, scanning electron microscope (SEM, SU8010), NT-MDT Prima scanning probe microscope, transmission electron microscope (TEM, Joel 2100F) and high-resolution TEM (Tecnai F 20). IR spectra were measured using a Fourier transform infrared spectrometer (FTIR, Nicolet 6700). XPS measurements were performed on a Thermo ESCALAB 250XI XPS Scanning Microprobe. Thermogravimetric (TG, 1100SF) analyses were measured with a heating rate of 10 °C min-1 between 30 and 900 °C under N_2 atmosphere.

Electrochemical performance test

All electrochemical tests were carried out in a three-electrode system using a CHI660E electrochemical workstation (Shanghai Chenhua, China). A Pt wire and an Hg/HgO electrod were used as the counter electrode, reference electrode and glassy carbon electrode modified with the corresponding catalysts was used as working electrode (surface area = 0.07cm^2). 6 μL as-prepared inks (5 g/L) were dropped onto the surface of the glassy carbon electrode (GC) and then dried under a fume hood for a few minutes. 5 mg of the above catalyst powders was dispersed in a mixed water and ethanol (1:1, v/v) solution 1.0 mL), respectively, and then 10 μL of Nafion solution (5.0 wt %) was added. Before the electrochemical tests, 1 M KOH solution

was bubbled by oxygen to reach the H_2O/O_2 equilibrium at 1.23 V vs. reversible hydrogen electrode (RHE) at room temperature. Meanwhile, before the electrochemical OER performance was tested, the electrode was pretreated via cyclic voltammetry (CV) scans at 100 mV/s to reach a stable state. The potentials measured were converted to the reversible hydrogen electrode (RHE) based on the equation $E_{RHE} = E_{Hg/HgO} + 0.059\ pH + 0.098$ V. Electrochemical impedance spectroscopy (EIS) measurements were recorded in the frequency range of 10^5–0.1 Hz with an amplitude of 5 mV under open-circuit potential. The double-layer capacitance (C_{dl}) of the sample was measured by cyclic voltammetry. Capacitive current densities were determined in the potential region 0.14 to 0.26 V versus Hg/HgO at the scan rates 20, 40, 60, 80, and 100 mV s^{-1}. The overall water splitting performance of the sample as both anode and cathode catalysts was constructed under 1.0 M KOH electrolyte.

Table S1. Crystal data for the CS, FS and CFS.

Compound	$Co_3(SeO_3)_3(H_2O)$	$Fe_2(SeO_3)_3(H_2O)_3$	$Co_3Fe_2(SeO_3)_6(H_2O)_2$
Space Group	*P* -1 (No.2)	*R* 3 c (No.161)	*P* -1 (No.2)
a (Å)	8.102(2)	9.360(1)	6.520(2)
b (Å)	8.219(2)	9.360(1)	7.995(3)
c (Å)	8.572(2)	20.297(2)	8.774(4)
α (°)	69.15(1)	90.00	85.51(2)
β (°)	62.88(1)	90.00	78.77(1)
γ (°)	67.23(1)	120.00	75.84(1)
Volume V/Å^3	457.12(20)	1539.98(36)	434.84(29)
Δd Co_1-O_6	0		
Co_2-O_6	0.0972		
Δd Fe-O_6		0.1538	
Δd $CoFe_1$-O_6			0.0301
$CoFe_2$-O_6			0.1113

Table S2. Comparison of OER activities for the as-prepared electrocatalysts in this study in 1.0 M KOH solution.

Catalyst	Mass activity at η = 0.35 V (A g^{-1})	Onset overpotential (V vs RHE)	Tafel slope (mV dec^{-1})
IrO_2	55.4	0.265	83.0
CS	68.1	0.269	66.7
FS	18.0	0.311	89.6
CFS	253.7	0.225	45.6

Table S3. Comparison of the OER performance of CFS with reported catalysts in alkaline solution.

Catalyst	Electrolyte	Substrate	Overpotential at 10 mA/cm^2 (mV vs.RHE)	Tafel slope (mV dec^{-1})	Reference
CFS	**1M KOH**	**GC**	**257**	**45.6**	**This work**
KCFS	1M KOH	GC	274	45.6	Chemical Engineering Journal 399 (2020) 125799.
CoPi-HSNPC-800	1M KOH	GC	320	85	ACS Sustainable Chem. Eng. 2019, 7, 13559−13568.
$CoMoP_2$	1M KOH	GC	270	51	J. Mater. Chem. A, 2020, 8, 2001-2007.
Cu-14-Co_3Se_4/GC	1M KOH	GC	280	111	ACS Catal. 2019, 9, 10761−10772.
FeCoMo-Se	1M KOH	CC	264	33	J. Mater. Chem. A, 2020, 8, 7925-7934.
Co−OH−HPi	1M KOH	GC	290	82	ACS Sustainable Chem. Eng. 2019, 7, 3083−3091.
$CoSe_2$/$FeSe_2$ DS-HNCs	1M KOH	NF	240	44	Nanoscale, 2019, 11, 10738–10745.

CoNC-NB2	1M KOH	RRDE	350	98	Small 2020, 2001171.
NCoBPi-PVP-450	1M KOH	GC	276	55.8	ACS Sustainable Chem. Eng. 2019, 7, 13981−13988.
$CoSe_{2-x}$-Pt	1M KOH	GC	255	31	Adv. Mater. 2019, 31, 1805581.
$(Co_{0.21}Ni_{0.25}Cu_{0.54})_3Se_2$	1M KOH	Au-coated glass substrate	272	53.3	J. Mater. Chem. A, 2019, 7, 9877-9889.
$Co(S_{0.22}Se_{0.78})_2$	1M KOH	NF	283	65.6	Adv. Funct. Mater., 2017, 27,1701008.
FeOOH(Se)	1M KOH	FF	287	54	J. Am. Chem. Soc., 2019, 141, 7005-7013.
CoZn-Se	1M KOH	GC	320	66	ACS Nano, 2019, 13, 5635-5645.
(Co, Ni)Se_2–NC	1M KOH	EG	258	73.3	Nano-Micro Lett. (2019) 11−67.
Co-$MoS_{1+X}Se_{1+Y}$	1M KOH	GC	280	71	Applied Surface Science 513 (2020) 145828.
SyA-Co_2Fe-ST	1M KOH	GC	254	50	ChemSusChem 2020, 13, 1–8.
$CoSe_2$-30	1M KOH	GC	287	54.3	Applied Surface Science 504 (2020) 144368.
$Ni_{0.6}Co_{0.4}Se$	1M KOH	NF	249	53	Nanoscale, 2020, 12, 4426–4434.
Au_1-$CoSe_2$	1M KOH	GC	303	42	Small, 2019, 15, 1805064.
Fe_7S_8 sheet	1M KOH	GC	270	43	J. Mater. Chem. A, 2019, 7, 22307.
CC/CNTs@$CoS_xSe_{2(1-x)}$	1M KOH	CC	285	63.3	ChemSusChem, 2019, 12(16): 3792-3800.
CoF_2	1M KOH	GC	285	60	Chemical Engineering Journal 397 (2020) 125500
CoFeO@BP	1M KOH	GC	266		Agewandte Chemie International Edition. Chem. Commun.
NiCoFeP/C	1M KOH	NF	270	65	2019, 55, 10896-10899.

Table S4. The electrochemical impedance at Open Circuit Potential in this work.

Catalyst	electrolyte resistance (R_s)	Charge transfer resistance (R_{ct})
CFS	4.938	1.481
CS	4.916	4.525
FS	5.422	6.972
IrO_2	8.473	3.455

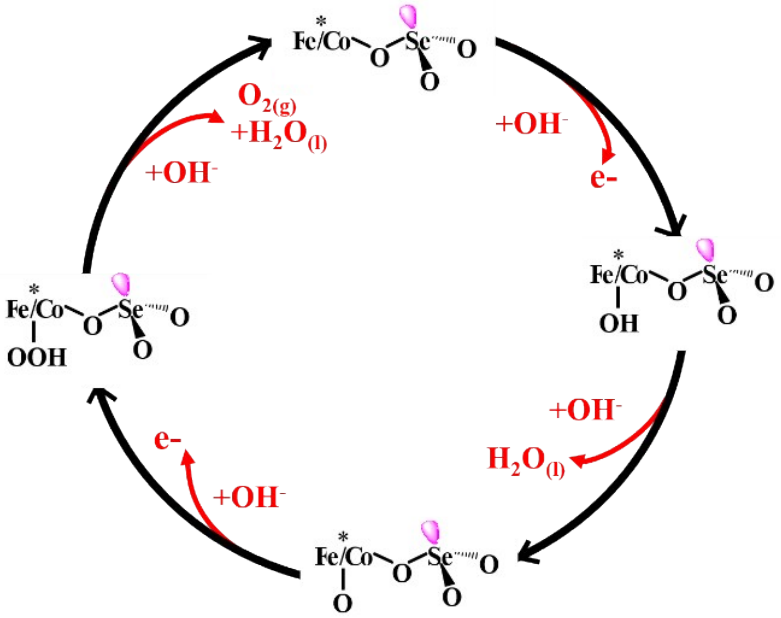

Scheme S1. The proposed mechanism for OER in basic medium of CFS. (* and purple ellipsoid represents active center and lone-pair electron, respectively).

Notes: The proposed mechanism for OER in basic medium was shown in Scheme S1, which follows the four-electron transfer process as shown in:

$$OH^- + M^* \leftrightarrow M-OH^* + e^-$$

$$M-OH^* + OH^- \rightarrow M-O^* + H_2O + e^-$$

$$M-O^* + OH^- \leftrightarrow M-OOH^* + e^-$$

$$M-OOH^* + OH^- \leftrightarrow O_2 + M^* + H_2O + e^-$$

Where M*, M-OH*, M-O* and M-OOH* represents the active sites and the intermediates (OH, O, OOH) adsorbed at the active sites，in addition, the SeO_3 anions with lone-pair electron might be easily adsorbed onto bimetallic active centres and increase the covalency between the metal and O atoms, accordingly, enhancing the activity of catalysts via the coordination interactions.

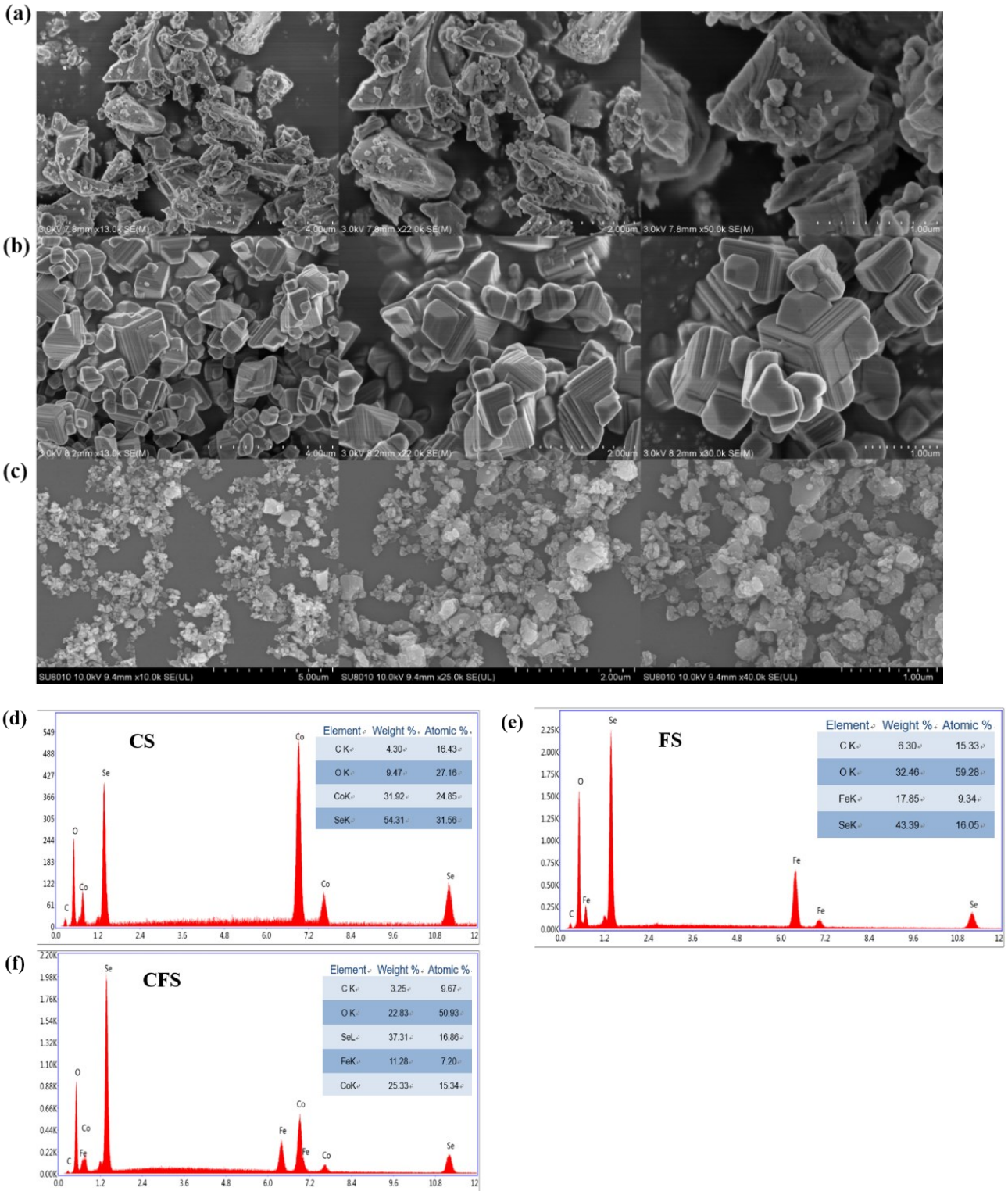

Figure S1. The SEM images of (a) CS, (b) FS and (c) CFS; EDX patterns of (d) CS, (e) FS and (f) CFS.

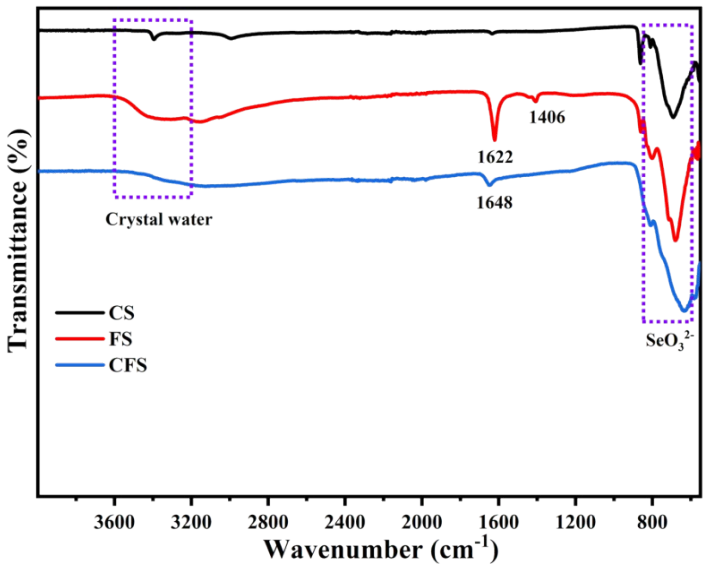

Figure S2. FT-IR spectra of CS, FS and CFS.

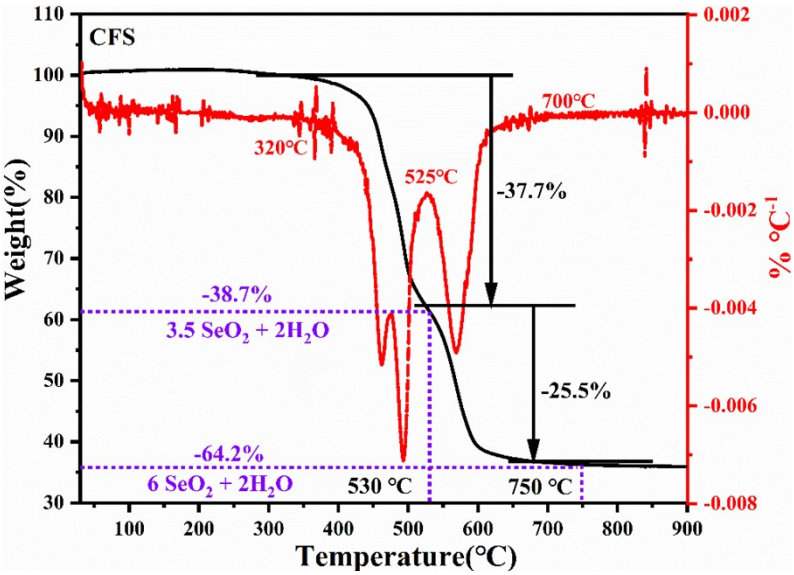

Figure S3. TGA and DTA pattern of CFS.

Notes: From TGA (Fig. S4) in a nitrogen atmosphere, the decomposition of CFS between 30-900 ℃ could be found, CFS could maintain its original structure before 320℃, as the calcination temperature increased, the CFS started to decompose, there was a total weight loss of 37.7 wt% from 320 °C to 525 °C, corresponding to the removal of partial SeO_2 and two water molecules per formula unit, and when the calcination temperature further rised to 700℃, a total weight loss was 63.2 wt% from 525 °C to 700 °C, which was ascribed to the removal of more SeO_2, thus, the final phase might be Co or Fe oxides.

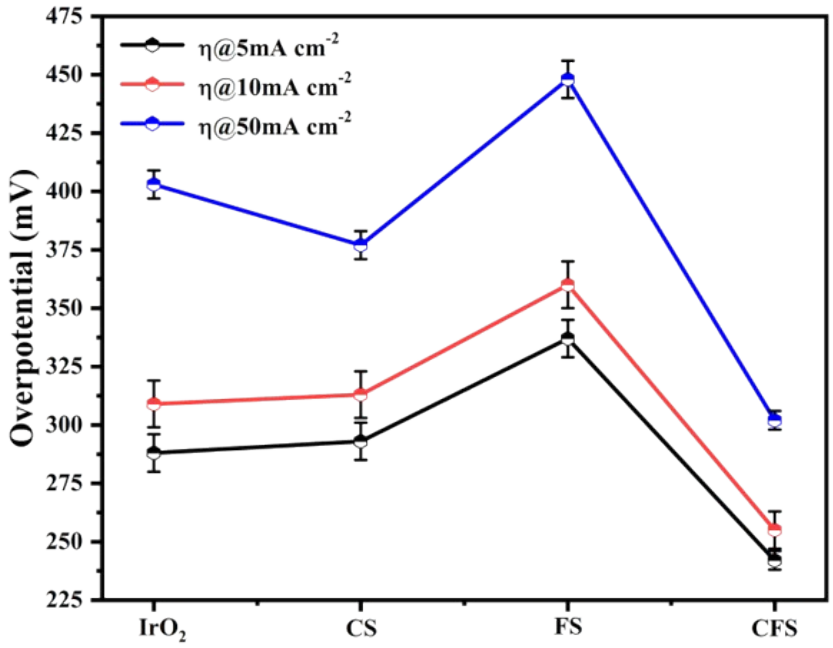

Figure S4. Comparison of overpotential at different current density of IrO_2, CS, FS and CFS.

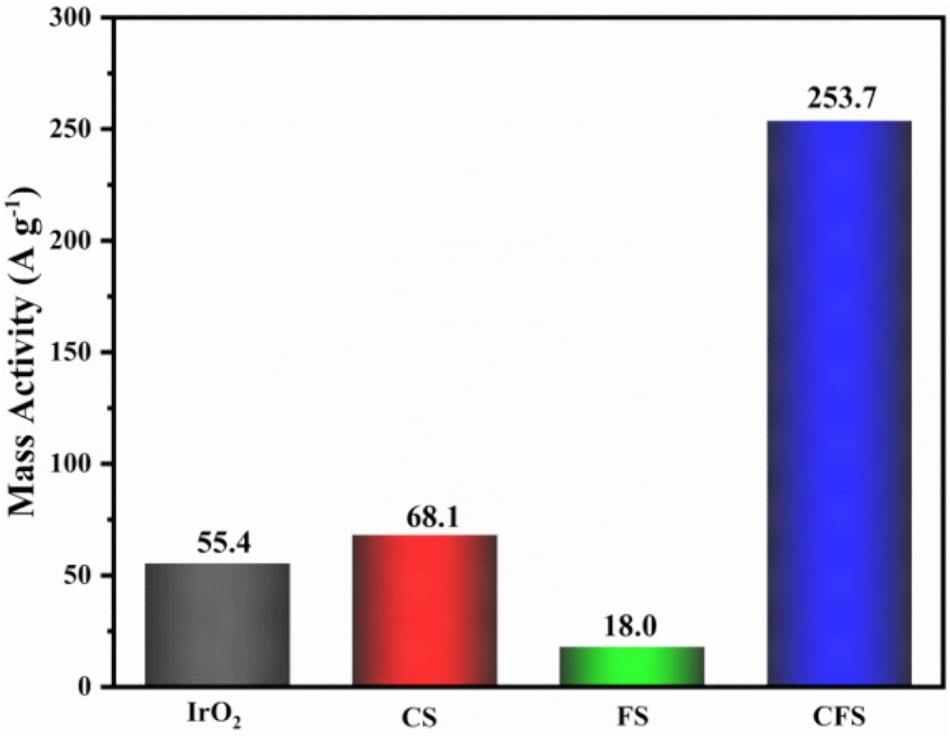

Figure S5. The values of mass activity (A g^{-1}) of IrO_2, CS, FS and CFS of current density j (mA cm^{-2}) at η = 350 mV.

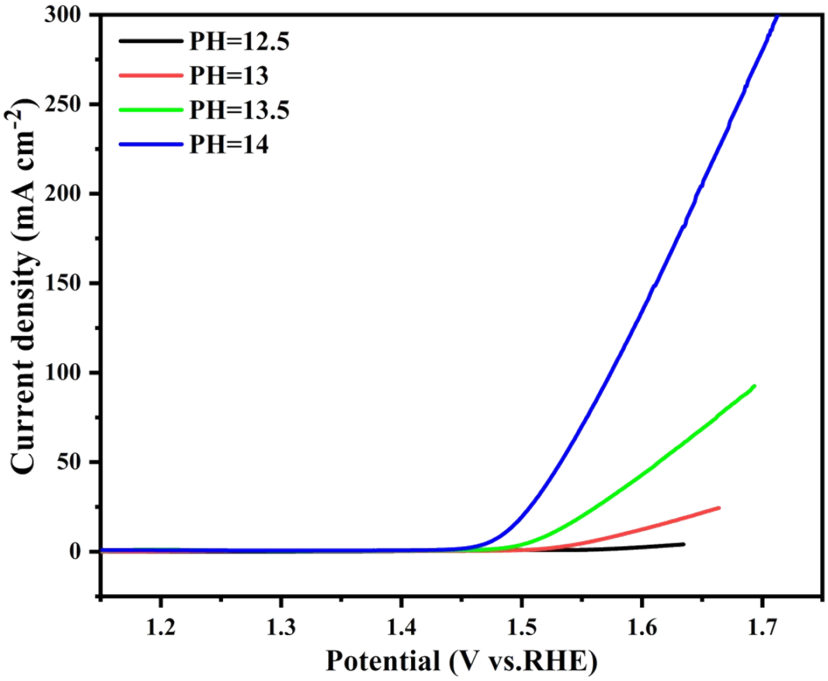

Figure S6. OER polarization curve of CFS at various pH.

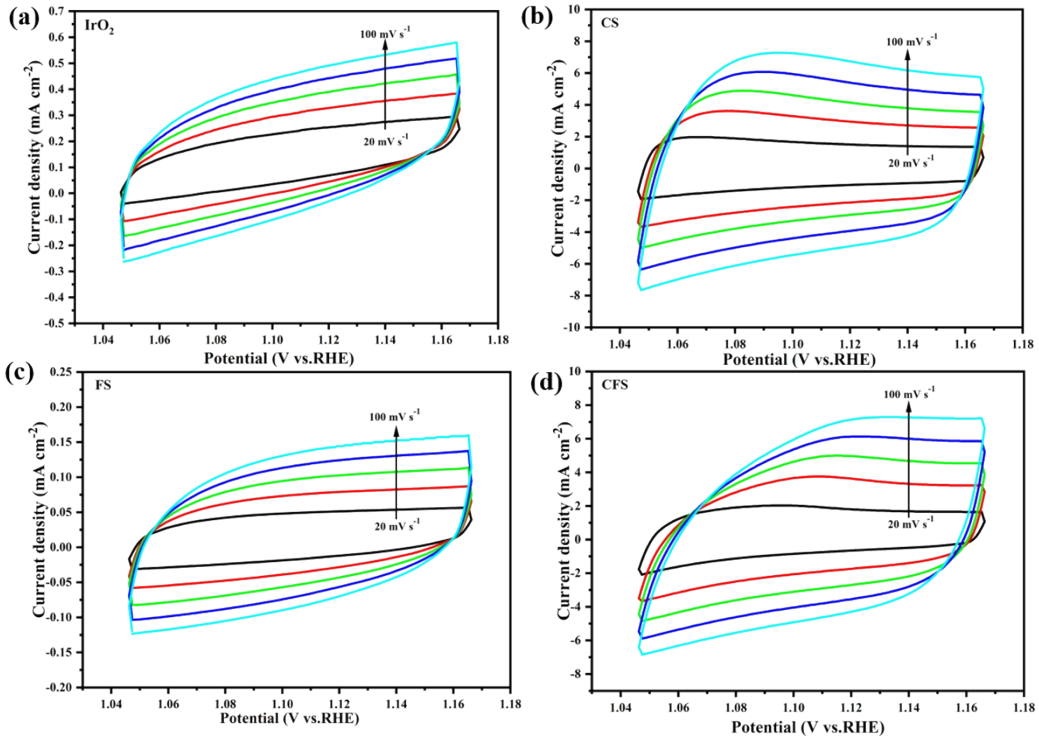

Figure S7. Cyclic voltammograms of (a) IrO_2, (b) CS, (c) FS and (d) CFS at different scan rates from 20 to 100 mV s^{-1}.

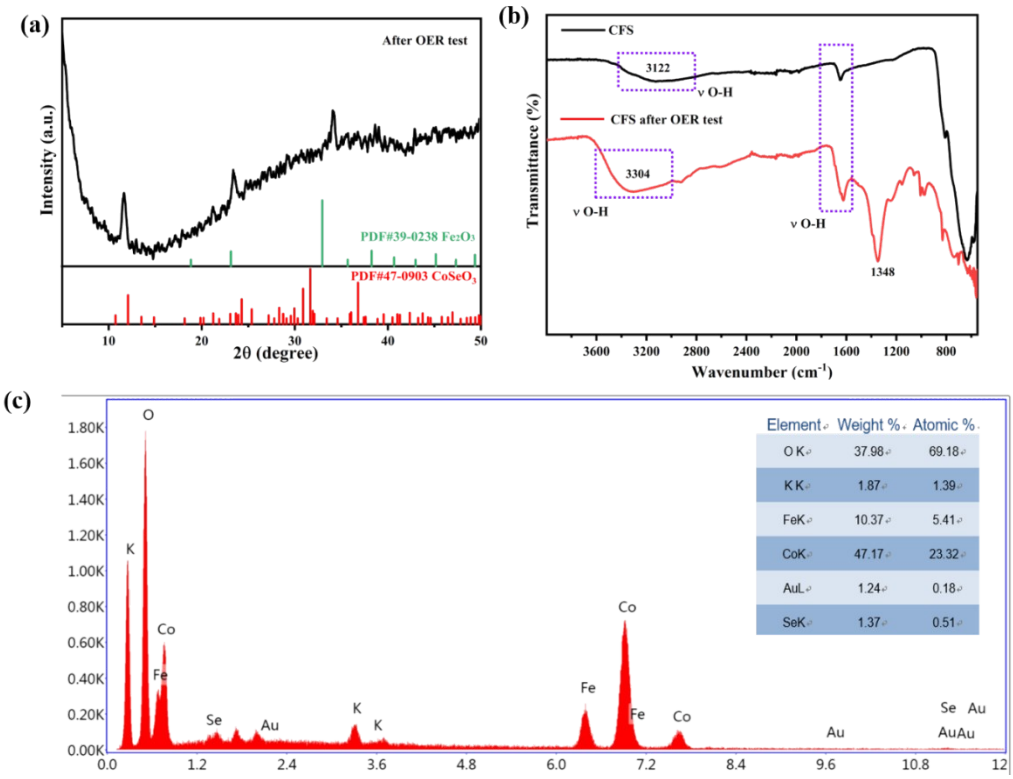

Figure S8. (a) The XRD patterns, (b) FT-IR spectra and (c) EDX pattern of CFS after OER test.

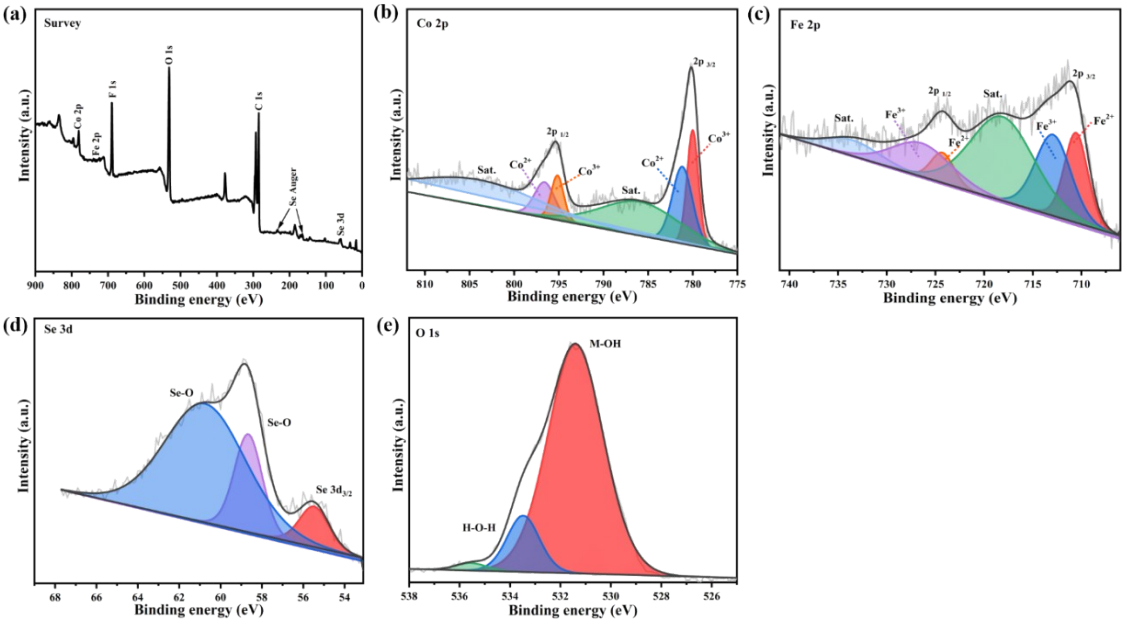

Figure S9. The XPS spectra of the CFS after OER test. (a) survey, (b) Co 2p, (c) Fe 2p, (d) Se 3d and (e) O 1s.

Notes: According to the fitting result of XPS, the content of Co^{3+} $2p_{3/2}$ and Co^{3+} $2p_{1/2}$ before OER was 7.53% and 4.88%, respectively. While, after OER, the content of Co^{3+} $2p_{3/2}$ and Co^{3+} $2p_{1/2}$ was 13.25% and 5.59%, respectively, indicating a significant increase of Co^{3+} after OER test, which should be attributed the formation of higher valence Co^{3+} on the surface of the CFS during this oxidation reaction.

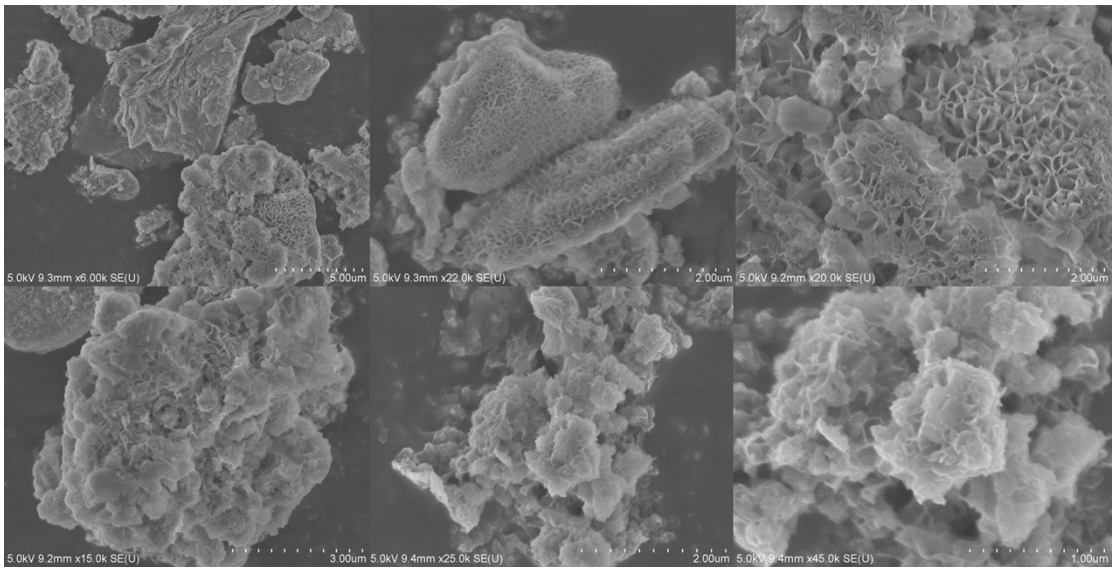

Figure S10. SEM images of the CFS after OER test.

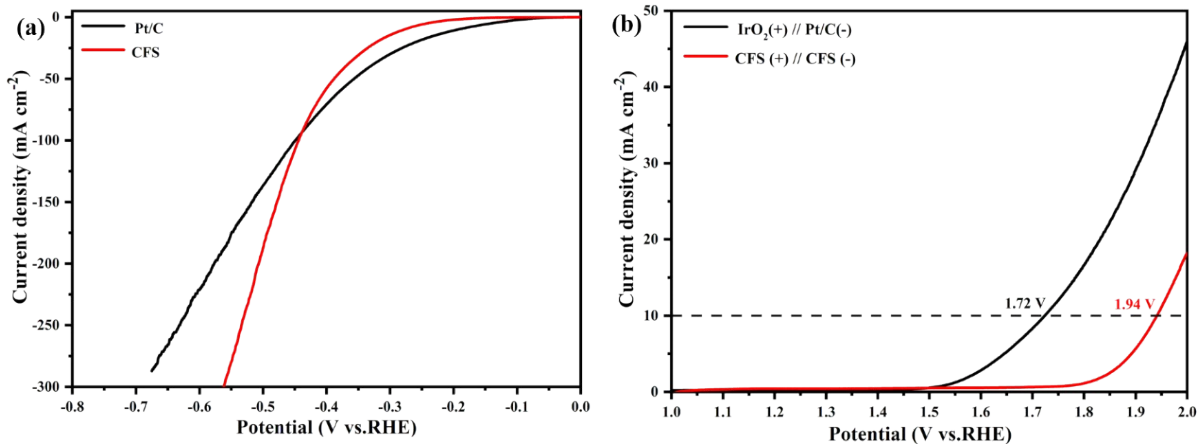

Figure S11. (a) HER polarization curve of CFS and (b) Polarization curve for overall water splitting with the CFS electrode as both the anode and cathode. sweep rate: 5 mV s^{-1} in 1.0 M KOH.